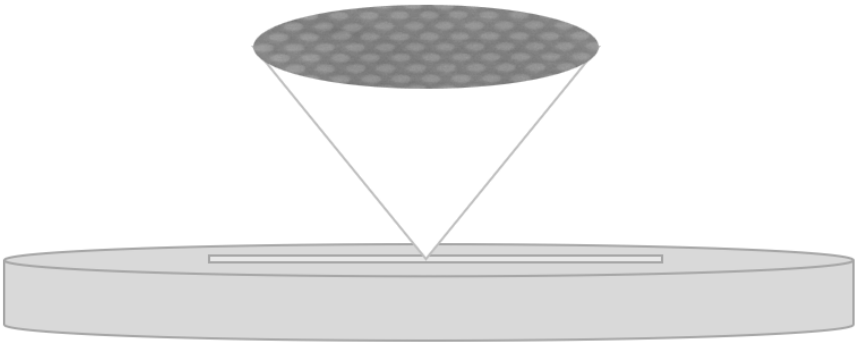

Nanofabrication of 2D Photonic Crystals for PCSELs emitting in UV region

Etching of wide bandgap materials to create 2D Photonic Crystals

Master's thesis in Nanotechnology

VISMAYA SUNIL

DEPARTMENT OF MICROTECHNOLOGY AND NANOSCIENCE

CHALMERS UNIVERSITY OF TECHNOLOGY
Gothenburg, Sweden 2024
www.chalmers.se

Master's thesis 2024

Nanofabrication of 2D photonic crystals for PCSELs emitting in UV region

A systematic study on various etching techniques and their effects on various compositions of AlGaN which is used to create devices that lase in UV region

Vismaya Sunil

CHALMERS
UNIVERSITY OF TECHNOLOGY

Department of Microtechnology and Nanoscience
Photonics Laboratory
Wide bandgap optoelectronics
Chalmers University of Technology
Gothenburg, Sweden 2024

Nanofabrication of 2D Photonic Crystals for PCSELs emitting in UV region
A systematic study on various etching techniques and their effects on various compositions of AlGaN for PCSELs emitting in the UV region
VISMAYA SUNIL

Examiner: Åsa Haglund, Photonics Laboratory
Supervisor: Doğukan Apaydin, Photonics Laboratory

Master's Thesis 2024
Department of Microscience and Nanotechnology
Photonics Laboratory
Wide bandgap optoelectronics
Chalmers University of Technology
SE-412 96 Gothenburg
Telephone +46 31 772 1000

Cover: Photonic Crystal

Typeset in LaTeX
Printed by Chalmers Reproservice
Gothenburg, Sweden 2024

Nanofabrication of two-dimensional Photonic Crystals for photonic crystals Surface-Emitting Lasers Emitting in the UV region
A systematic study on various etching techniques and their effects on various compositions of AlGaN which is used to create devices that lase in UV region
VISMAYA SUNIL
Department of Microtechnology and Nanoscience
Chalmers University of Technology

Abstract

Lasers are light sources that produce coherent beams. Semiconductor lasers offer notable advantages such as compact size, lower power consumption, and extended lifespan over other laser types. Among different semiconductor lasers, photonic crystal surface-emitting lasers (PCSELs) are recognized for their high optical output power and low beam divergence, achieved through the use of a two-dimensional photonic crystal. The proposed PCSELs use photonic crystals which offer refractive index contrast in two dimensions. This creates a standing wave with zero group velocity and vertical emission through Bragg diffraction. PCSELs have been successfully demonstrated in the visible and infrared wavelengths, but not yet in the ultraviolet (UV) range. This gap represents a significant opportunity, as UV-emitting PCSELs find potential applications in lithography, sterilization, and processing of materials. This project aims to explore different etching techniques to deep into the cladding layer of the PCSELs. To keep the optical losses low, the vertical field profile should not overlap with the absorbing metal layer used for the p-contact. Therefore the distance between this metal and the QWs needs to be large and on the order of 300-400 nm. The bottom of the photonic crystal holes on the other hand should be very close to the top QW (about 60 nm). To fulfill both these requirements the photonic crystal should have an etch depth of about 300 nm. Etching is preferred over alternative methods, such as over-growth or mass transport, due to its presumed simplicity and cost-effectiveness.

Keywords: Photonic crystal, Etching, ICP-RIE, UV Lasers, AlGaN, PCSEL

Acknowledgements

The last two years and especially the last five months have been a period of growth and learning that makes me proud of the person I have become. At least for now.
My examiner, Åsa Haglund is a testament to the fact that kindness and empathy make the best teams challenging the stereotypical notions of leadership. Dogukan Apaydin, my supervisor and mentor, ensured that I learned and understood the project while answering the same question for the hundredth time and showing the same patience as he did for the first time.
I am also extremely grateful to have the people in the Photonics Laboratory around me who have made my time at MC2 fun, comfortable, and memorable, with special thanks to Gunnel, for making my arrival and settling to Chalmers easy, to Estrella, for helping me out with the electrical conductivity measurements, and to Phuc, for his valuable insights on my process and results. This thesis would not have been the same without the reassurance and joyful company of the other Master's thesis students, especially Elin and Tin Tin.
My experiments could not have been complete without the use of the Myfab nanofabrication lab and the members who ensured the successful completion of the experiments. I am extremely thankful to Ruggero Verre who has given me valuable insights on the plasma-based dry etching process and who was invested to see that I reach my objective successfully.
I also thank my family for supporting me throughout my master's education and my entire life, even though sometimes we don't see eye to eye. I also thank my friends who have stuck with me through thick and thin, my people in Stockholm, and my people in Gothenburg, I don't think I would have made it without you.

Vismaya Sunil, Gothenburg, June 2024

List of Acronyms

Below is the list of acronyms that have been used throughout this thesis listed in alphabetical order:

AlGaN	Aluminium gallium nitride
AlN	Aluminium nitride
Ar	Argon
BSE	Back-scattered electrons
Cl_2	Chlorine
ICP RIE	Inductively Coupled Plasma Reactive Ion Etching
PCSEL	Photonic Crystal Surface Emitting Lasers
PMMA	Polymethyl methacrylate
RF	Radio frequency
SE	Secondary electrons
SEM	Scanning Electron Microscopy
TMAH	Tetramethylammonium hydroxide

Contents

List of Figures

List of Tables

1

Introduction

Ultraviolet (UV) light has applications in communication, water purification, lithography, plant lighting, sterilization, and medical treatments. For wavelengths from 100 nm to 400 nm, UV technology has traditionally relied on mercury lamps. While these lamps generate a broad UV spectrum for various uses, they have drawbacks such as environmental concerns, high energy consumption, and limited lifespan [1]. Their bulky, fragile nature also complicates modern system designs. Although UV light from the sun exists, the UVC component is absorbed by the ozone layer, making it difficult to harness. Lasers have a long history, with the theoretical foundations established in 1917 [2]. Since then, laser technology has advanced, leading to the development of various types, including semiconductor lasers, which are essential to modern applications. These advancements have broadened laser uses, from scientific research to industrial processes [3]. Today, lasers are crucial in fields like industrial manufacturing for cutting, welding, and engraving. In medicine, lasers are used in surgeries and treatment therapies. Semiconductor lasers offer advantages like no warm-up time, reduced waste, compactness, and long operational life [4]. Surface-emitting lasers are preferred for their long life, high power efficiency, and easy integration with optical fibres [5, 6]. Their compact design allows them to fit into a wide range of devices, from portable medical tools to industrial machinery, without sacrificing performance. One promising advancement in laser technology is photonic crystal surface-emitting lasers (PCSELs), which are considered strong candidates for UV sources. They offer high brightness, crucial for applications like photolithography, and eliminate the need for bulky external optics by generating a focused, directional beam within the photonic crystal structure, reducing system complexity and cost [7]. PCSELs combine high output power, excellent beam quality, and precise beam control, making them suitable for a wide range of applications [8]. While PCSELs emitting in blue and green parts of the visible spectrum have been demonstrated, UV PCSELs remain underexplored [9]. Their development could transform fields like biotechnology, enabling advanced imaging and new diagnostic tools. Compact, efficient UV PCSELs could also open new possibilities in environmental monitoring, allowing portable UV sources to detect pollutants in air and water [10]. This project aims to optimize the fabrication of photonic crystals for UV PCSEL lasing by refining etching techniques, eliminating the need for re-growth or wafer fusion, thus simplifying the process and reducing costs [11]. Achieving high-quality photonic crystals is crucial for efficient and reliable UV PCSELs, requiring precise control over fabrication. Key objectives include achieving a favourable aspect ratio of the holes in the photonic crystal and depositing a thick metal layer for efficient electrical pumping. The filling factor of a PCSEL affects the band structure

and the coupling of diffracted light in the PCSEL [12]. A high aspect ratio is required to achieve the desired filling factor at the bottom of the photonic crystal where the mode overlap is the highest. It also allows better control over the filling factor at the bottom of the photonic crystal, where mode overlap is greatest, affecting modal losses and the lasing threshold [13]. Meanwhile, a thick metal layer is essential for efficient electrical pumping. This thesis aims to aid with the fabrication of UVC PCSELs using etching. Overgrowth methods with buried SiO_2, mass transport, and wafer fusion techniques have been used to fabricate PCSELs. However, the SiO_2 layer creates a weak resonance effect as the refractive index contrast is not high and the fabrication is complicated. The mass transport technique has been shown to deteriorate the uniformity of the semiconductor-air interface in the PhC [9]. Etching holds a promising approach as it has already succeeded in creating PCSELs emitting in the green region of the spectrum [11]. Since the photonic crystals are on top of the quantum well, it is less complex and does not cause degradation to the quantum well due to regrowth. However, there exists a potential for etch-induced damage to quantum wells. The target etch depth is 300 nm to avoid optical absorption by metal and to prevent etch-induced damage to quantum wells. By optimizing etching techniques, this project aims to advance UV laser technology by fabricating UVC-emitting PCSELs that are estimated to have 50W performance output power and beam divergence of less than one degree. In order to achieve this, structures with an aspect ratio close to 1:10 need to be etched in III-nitride materials, while ensuring the etched structures have smooth side profiles.

2

Background

This chapter intends to summarize the key concepts that were used to understand the physics behind the device being fabricated. The basic ideas that underpin the creation of PCSELs are presented in this chapter. We start by discussing the working principles of lasers, the properties of photonic crystals and specifically 2D photonic crystals, and the basic properties of $Al_xGa_{1-x}N$ and end by describing the proposed design of the PCSEL.

2.1 Stimulated emission and Lasers

LASER stands for Light Amplification by Stimulated Emission of Radiation, and as its name suggests is a light source that emits coherent radiation by stimulated emission of photon. This is possible when population inversion is established by current injection or optical pumping. Optical gain and feedback are two requirements to build a laser. Lasers produce highly concentrated beams of coherent light through stimulated emission. They operate based on the principles of quantum mechanics, particularly the interaction of electrons within atoms or molecules. The radiative transition is a process where a photon is emitted when the electron moves to a lower energy state. They are divided into stimulated and spontaneous transitions. When an electron in the conduction band makes a transition to an empty valence band state stimulated by an incoming photon, it's called stimulated emission as depicted in Figure 2.1. If all the photons emitted by the transition have the same frequency, phase, and direction of propagation, then it is called coherent radiation. In contrast, spontaneous emission occurs when an electron transitions to a lower energy state without external stimulation, emitting photons randomly in all directions. While spontaneous emission is responsible for the initial generation of light in a laser, it is the process of stimulated emission that amplifies this light, leading to highly coherent emission. A laser consists of an optical gain medium, pump, and optical resonator. The pump is the energy supply that establishes population inversion. The optical gain medium is where the population inversion and the subsequent, radiation occur from. The optical resonator ensures that necessary feedback is provided. Various types of lasers exist, including gas, solid-state, and semiconductor lasers, each with distinct gain media and operational mechanisms. They differ in terms of the material with which it is made and how the active media and the resonator are designed. Gas lasers, such as helium-neon and carbon dioxide lasers, use a gas-filled tube as the gain medium, with electrical currents or light used to excite the gas atoms. Solid-state lasers, on the other hand, use a solid crys-

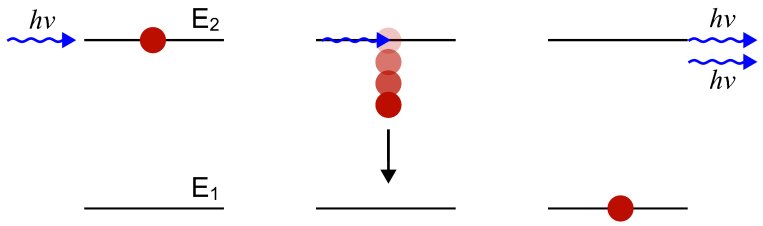

Figure 2.1: Simplistic model of stimulated emission of a photon from an atom. An incoming photon interacts with an electron at a higher energy level E2 which causes it to fall back to the lower energy level E1, during the process emitting two-photon having the same frequency, phase and direction of propagation. This starts off a chain reaction which enables emission.

tal, like ruby or neodymium-doped yttrium aluminium garnet, as the gain medium, with flash lamps or diodes providing the necessary energy. Each type of laser has specific applications depending on its wavelength, power, and beam quality. Unlike traditional lasers, semiconductor lasers offer improved performance and integration capabilities, addressing the demands for high output power and beam quality [14].

2.2 Photonic crystals and properties

Photonic crystals are structures that have periodic variations in refractive indexes. This causes a photonic bandgap analogous to the electronic bandgap to be formed. These structures can be designed so that a certain wavelength is confined. They are divided into one-dimensional (1D), 2D, and three-dimensional (3D) crystals depending on the number of directions in which the refractive index changes periodically. The different types are depicted in Figure 2.2. 1D photonic crystals, often realized as Bragg gratings, may not offer a complete photonic bandgap but are simpler to fabricate. On the other hand, 3D photonic crystals, while theoretically capable of offering a complete bandgap in all directions, are challenging to fabricate with current technology. Due to these fabrication difficulties, 2D photonic crystals are considered more appealing for practical applications, offering a good balance between performance and manufacturability. The development of 2D photonic crystals has also paved the way for compact and efficient lasers, modulators, and sensors, which are crucial for advancing photonic technologies. The photonic bandgap offered by the photonic crystal depends on several parameters, including the lattice constant, rod radius, and refractive index contrast. By carefully tuning these parameters, it is possible to design photonic crystals that selectively block or allow specific wavelengths, making them highly versatile in various applications. For instance, photonic crystals can be used in the design of highly efficient mirrors, known as distributed Bragg reflectors (DBRs), which reflect specific wavelengths while transmitting others. These mirrors are essential components in many laser systems, where they help to define

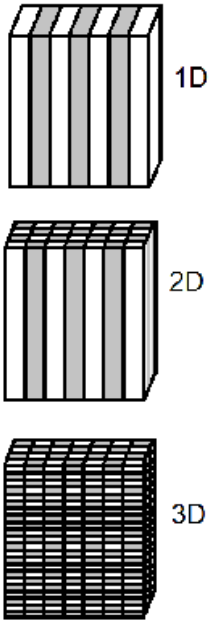

Figure 2.2: 1D, 2D and 3D photonic crystal structures [15].

the lasing wavelength and enhance the overall efficiency of the device. Photonic crystals offer high speed and low energy consumption due to their ability to manipulate light with minimal loss and without the need for electrical conversion. The concept of mirrorless feedback in photonic crystals achieved through Bragg scattering, is another area of interest. In this scenario, the periodic structure of the photonic crystal itself provides the necessary feedback for laser operation, eliminating the need for traditional mirrors. This approach can lead to the development of more compact and robust laser systems with fewer components and reduced complexity. The ability to restrict oscillation to a narrow spectral range through the design of the photonic crystal also allows for the creation of lasers with very precise wavelength control, which is crucial in applications such as high-resolution spectroscopy and optical sensing [16].

2.2.1 2D photonic crystals for PCSELs

The 2D photonic crystal structure in the PCSEL creates a 2D standing wave that is amplified in the active region to ensure that a laser beam of a single wavelength is emitted. This is possible as the 2D photonic crystal structure ensures the group velocity of the desired mode propagating over the entire surface is zero, hence creating a standing wave. Since the optical feedback is provided from the entire area of the crystal, it allows single-mode emission from a broader area. Then it ensures the emission of the desired mode in a direction normal to the surface, also termed the guided-wave mode, through Bragg diffraction [13]. In Figure 2.3, the curvature of the bands, as marked by the blue lines, corresponds to the group velocity of the guided-wave modes. Γ, X, M mark the high symmetry points in Figure 2.3, where the zero group velocity at the Γ points are highlighted. As there is no periodicity variation in the vertical direction, effective light out-coupling guarantees

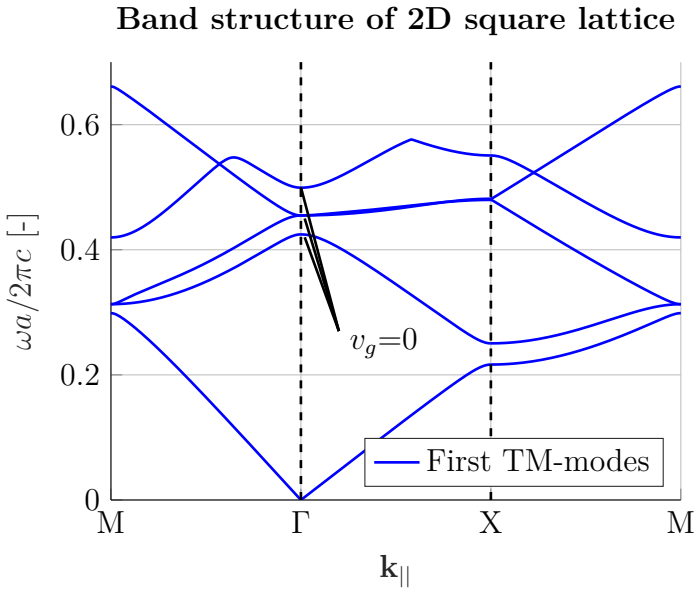

Figure 2.3: The photonic band diagram for a 2D photonic crystal in AlGaN with a square crystal lattice, a = 128.4 nm, and with a square air-hole, d = 55 nm [17].

single-mode emission over large regions and improves optical gain and coherence in devices such as photonic-crystal surface-emitting lasers (PCSELs). Precise control over the behaviour of light within the crystal is possible by varying the dielectric contrast, and the lattice geometry of the materials to tailor the spectral positions of the zero group velocity points.

2.3 III-nitrides for UV emitting PCSELs

The bandgap of the semiconductor determines the emission wavelength of semiconductor lasers. Hence to have emission in the UV region, the active region should include UV-emitting material and the rest of the structure should be UV-transparent. This is why $Al_xGa_{1-x}N$ is suitable for PCSELs emitting in the UV region. $Al_xGa_{1-x}N$ is a compound semiconductor. Compound semiconductors are the type of semiconductors that contain more than one atom from different groups of the periodic table. A typical semiconductor crystalline structure is defined by a lattice, a set of points that form a 3D periodic structure, and a basis, a group of atoms repeated at every lattice point. The lattice point has three lattice vectors. A unit cell is the smallest volume cell, which forms the entire crystalline structure when repeated in all directions. One of the basic unit cell structures is simple hexagonal as described in Figure 2.4. AlN crystallize in wurtzite structure. It is obtained by two overlapping hexagonal closed pack structures with a distance of 3c/8 between each other in the vertical direction, where c is the lattice constant in the z-direction. It can be also considered as a hexagonally closed-packed lattice with two basis atoms. The bonding forces are strong and equal in all directions, hence cleaving does not form atomically smooth surfaces. This is a challenge when vertical structures need to be evaluated by cleaving the sample. AlN is a binary compound semiconductor

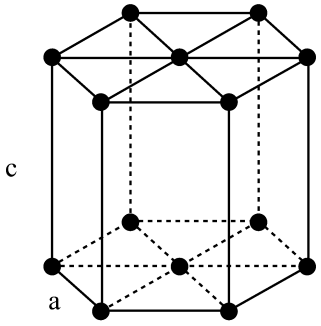

Figure 2.4: Hexagonal lattice structure. The distance between the nearest neighbours is marked by a and the lattice constant in the z direction is marked by c [18].

with elements from III-V groups of the periodic table. The lattice constant of the crystalline structure is around 3.1 Å, the bandgap energy is close to 6 eV, and the emission wavelength is close to 200 nm. This makes it a suitable choice for the cladding layers in an optically pumped UV laser. Hence the photonic crystal layer is made from AlN and the layers below the photonic crystal are made from various forms of $Al_xGa_{1-x}N$. The lattice constant a varies from 0.3110-0.3113 nm and c from 0.4978 nm-0.4982 nm. The c/a ratio is 1.633 which is caused by the ionic nature of the bonds which in return provides the piezoelectric properties[19][20].

2.4 Photonic crystal surface-emitting lasers

PCSELs are optoelectronic devices that enable lasing with low divergence and high output power. Photonic crystals enhance the directionality and coherence of laser beams by limiting the range of wavelengths at which light may form a 2D standing optical field by ensuring zero group velocity and effective outcoupling of the desired mode. Hence, PCSELs can produce higher output powers with symmetric, low-divergent beams without the use of external lenses. The surface emission simplifies integration into photonic systems and improves performance in applications such as sensing, displays, and communications. To provide a working lasing, PCSELs integrate multiple components that operate in harmony. The active layer produces light and optical gain and is usually made up of quantum wells. Light is helped to be contained vertically by the top and lower cladding layers that surround this layer. The intended PCSEL design is depicted in Figure 2.5 and its 3D view is in Figure 2.6. Surface emission is produced when light from the active layer interacts evanescently with the photonic crystal layer. PCSEL uses a two-dimensional (2D) photonic crystal. A zero in-plane group velocity can be produced by the 2D photonic crystal for the guided-wave modes that travel across the surface, which generates the necessary optical input from coupled fields across the entire crystallographic area. The single-mode stability of these guided-wave modes encompasses a wider region, enabling the PCSEL to have a broad mode while maintaining single-mode emission

[3].

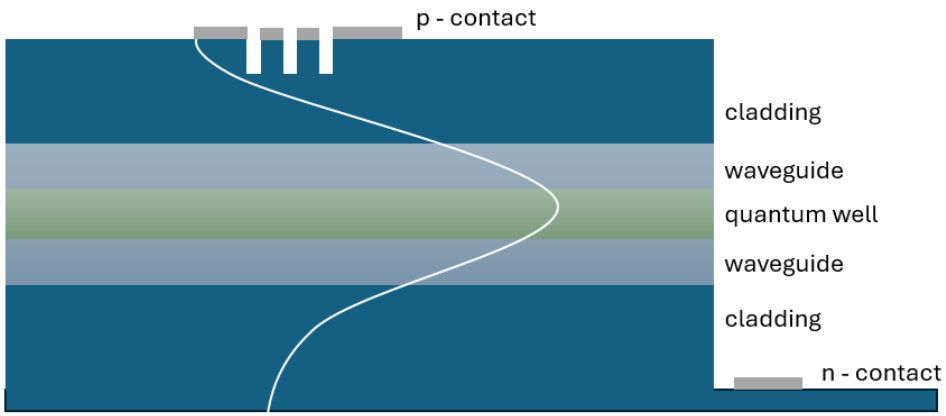

Figure 2.5: Photonic crystal surface-emitting laser in cross-sectional view with contacts for electrical injection.

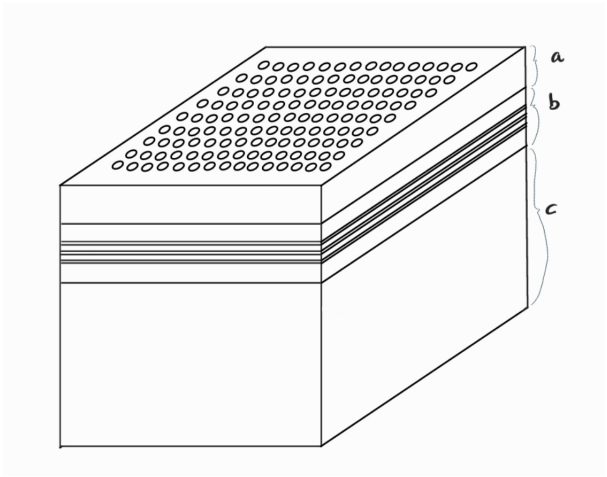

Figure 2.6: A sketch of the 3D view of a PCSEL; a) photonic crystal b) multiple quantum wells in waveguide c) substrate with cladding.

3

Nanofabrication of 2D photonic crystals

The PCSEL for ultraviolet-C emission has been grown on a sapphire substrate with Aluminium Nitride cladding. The core consists of multiple quantum well structures which are composed of $Al_{0.3}Ga_{0.7}N$ with $Al_{0.7}Ga_{0.3}N$ waveguide. The nanofabrication should be able to yield the desired structure by adhering to the following conditions-

- A thin AlN layer is grown, into which cylindrical air gaps are etched to form the photonic crystal
- The depth of the cylindrical air gaps needs to be around 300 nm deep. This helps to reduce the absorption of the mode by the metal layer as depicted in Figure 3.1 as there is sufficient physical distance between the active region and the metal layer.
- The aspect ratio between the depth of the cylindrical air column and the diameter of the same needs to be at least 1:10.
- A metal layer has to be deposited to explore the electrical pumping of the device which also needs to act as the sacrificial layer for the etch process.

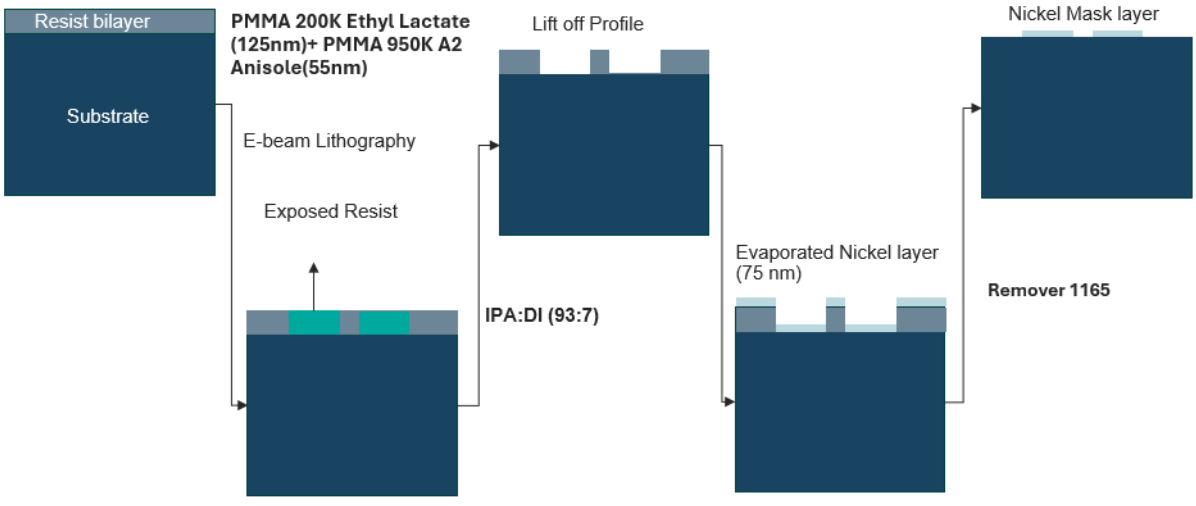

Figure 3.1: Overview of the fabrication of PCSEL structure to be etched.

The steps involved in the fabrication are outlined in Figure 3.1. This section will describe the steps involved in the creation of the photonic crystal structure as per the requirements and the various techniques used in detail. The resist PMMA was added

with the two layers. This is because the two of them have different sensitivities, so there is an undercut. This ensures proper liftoff. The photonic crystal structure required to act as the reflector for the device comprised an AlN layer with air gaps of 30 nm diameter and 300 nm depth, with a Ni layer on top.

3.1 Patterning

To create the required structure in the AlN layer, we need to transfer the pattern onto it. The scale of the dimensions of the required patterns is smaller than the resolution of optical lithography. Hence e-beam lithography is used as it is applicable for the feature size of the design. The pattern produced on the AlN layer is used as the mask for further processing.

3.1.1 E-beam lithography

E-beam lithography uses an electron source to produce a beam which is used to get the desired pattern on the layer. For this purpose, a positive tone high-resolution e-beam resist PMMA is first coated onto the surface. The beam is exposed to the region that needs to be removed, one pixel at a time. To obtain this electron beam with a small spot size, The electron stream is usually produced by either thermionic emission, field emission, a combination of both, or photoemission. The electrons generated are then condensed into a beam with a small spot size using a series of electrostatic lenses. The disadvantage of e-beam lithography is its decreased throughput [21]. For the subsequent etching, a mask is required. This mask has to be resistant to reactive ion etching. PMMA does not have sufficient resistance to dry etching, a metal mask may be necessary. Since the device is meant to be electrically driven, it gives more incentive to deposit a metal layer on the top of the photonic crystal layer. However, the metal shouldn't be inside the air rods as it can lead to absorption of the modes, hence the metal needs to be deposited before the etching process. While the possibility of depositing a metal layer after etching exists via tilting the sample, it introduces metal on the top part of the air gap which is not favourable. Further, the tilt angle and air gap hole size become additional parameters in the process which increases the complexity of the process and is beyond the scope of this thesis. One of the ways to overcome this bottleneck is to use the metal layer needed for the electrical pumping as the mask. To ensure the metal is deposited as the mask, the liftoff technique is used rather than etching as this would require an additional e-beam lithography step which is difficult as we need to make sure that the underlying patterned resist is aligned with the resist pattern on top of the metal layer. While this is theoretically possible, it is difficult to achieve realistically as there could be misalignment. Hence after the resist is patterned using e-beam lithography, the exposed region is removed, to enable further processing.

3.1.2 Lift-off

Lift-off is a popular technique for difficult-to-etch materials. The steps involve -

- Deposition of resist onto the substrate

- Patterning of resist, in this case using e-beam lithography
- Removal of the exposed region
- Deposition of the mask, in this case, nickel
- Immersion of the wafer to a remover that dissolves the resist, removing the metal layer deposited on top of the resist in the process

To enable successful lift-off as described above, the vertical edges should be intentionally not be covered by the metal to enable the remover to act on the resist. If good step coverage is enabled, then the metal layer will protect the resist from the remover. Sputtering is not ideal in this case as it provides good step coverage, however, evaporation serves well for this purpose. Evaporation is a process of metal deposition in which a crucible containing the target metal is heated. The pressure is kept low so that the vapours from the heated crucible, are collected and condensed on the target which is kept suspended above the crucible. Since the metal layer needs to be thick enough to not get wholly consumed by the etching process but thin enough to enable successful liftoff, 75 nm of nickel is deposited. This is because 180 nm thick resist is deposited and typically the metal layer should be less than half of the resist thickness. To wholly ensure that the metal is not deposited on the vertical sidewalls, an undercut in the resist is made by using two layers of resist with varying sensitivity to the e-beam. The resist with higher sensitivity is coated as the first layer and the resist with the lower sensitivity as the second layer, this ensures that the layer with the higher sensitivity is developed more compared to the other, producing an undercut where metal deposition via evaporation is highly unlikely. The resists are developed with IPA: DI water (93:7) mixture for 120 s.In this case, the first one is PMMA 200 K with ethyl lactate and the second one is PMMA 950K with anisole. We used PMMAs with different solvents to prevent intermixing when coating [21].

3.2 Etching

Etching is the process used to transfer patterns from a mask to the underlying layer. In this case, the mask used is nickel and the underlying material is AlN. The common figures of merits used to quantify the quality of the process are etch rate, selectivity, and undercut. Etch rate is the thickness of the material removed per unit of time. Selectivity is the ratio of etch rates between the mask and the etched layer, which makes it an important parameter to analyze the choice and thickness of the mask used. The etched sidewalls may not always be vertical hence analyzing the undercut, that is the lateral extent of the material removed, is also an important figure of merit. Etching can be divided into dry and wet etching. Physical and combination etching methods typically fall under dry etching and use plasma to generate chemically reactive species that react with the layer to form volatile by-products which are then easily removed. Wet etching is a purely chemical process where the sample is immersed in the etching solution which reacts to the areas not protected by the mask, which is typically inert to the solution, to be removed [21]. Dry etching consists of ion milling and plasma-based etching. Plasma-based etching is a type of dry etching that can involve both purely chemical attack or a combination of both chemical and physical etching. Plasma-based etching can be classified into different types depending on the nature of the discharge gas, the extent of the bombardment caused by the ion generated by the glow discharge, and the volatility of the gas process formed. Ion Milling is a purely physical etching mechanism. Ion-milling uses noble gases as the etch species, hence there is no chemical reaction involved. This process is highly directional but offers low selectivity as there is no chemical reaction involved and the process is purely mechanical. Reactive ion etching is a plasma-based process that shows higher selectivity than ion milling and, hence is considered a more promising candidate for the process, as the mask used is not removed after the process and is part of the device. Wet etching, which is also a purely chemical process, is highly selective but it comes at the cost of low anisotropy as the etchant solution attacks the exposed region uniformly, and poor process control as the process is limited by temperature dependence and solution particulate contamination [22].

3.2.1 Dry etching

The plasma-based processes are defined by these steps:

- Plasma generation: By breaking down the feed gas (in this case chlorine (Cl_2) and argon (Ar))into chemically reactive species. The feed gas when broken down consists of ions, radicals, electrons, and neutrals. Physical damage is caused by neutrals and also by ions. Chemical attack is dependent on ions and radicals.
- Adsorption: By diffusion of the chemically reactive species to the layer to be etched. The extent of the bombardment by the chemically reactive species is determined by the field near the substrate, which can be either null or extensive depending on the target electrode on which the sample is placed.
- Reaction: Chemically reactive species undergo surface diffusion to then react

with the exposed region. If inert gases are used, then the subsequent ion bombardment doesn't cause only physical damage.
- Desorption of reaction product and removal from near the substrate region: For etching to take place the reactive gas discharge from the plasma has to produce a volatile gas-surface product.

To understand the etch mechanism, it is crucial to analyze what might be the rate-limiting step. Depending on the nature of the gases, and the extensiveness of bombardment, the following plasma etching can be divided into the following as they are relevant to the experiments conducted [23].

3.2.1.1 Ion milling

Ion milling is done by physically damaging the substrate via ions accelerated toward the sample. For this purpose, inert gases are used to generate the plasma. When the ions are formed in the plasma they are accelerated towards the negatively charged cathode, during this motion the the ions may collide with neutral species. If the energy transfer is greater than the ionization energy of the molecule then the neutral atom becomes an ion, and further, all these ions bombard the cathode which causes the bonds in the top layer of the target to be broken. The process used a strong vertical electric field concerning the sample and low chamber pressure, which results in high directionality. The low pressure ensures minimal collisions between ions and gas molecules, thereby making the etch highly anisotropic.

3.2.1.2 Inductively coupled plasma RIE

The Oxford Plasmalab 100 Inductively Coupled Plasma/ Reactive Ion Etching is used for reactive etching. The nickel layer deposited by the liftoff process is used as the mask. The laser interferometer endpoint system is used to estimate the etch rate. The factors explored in the experiments are Electrode RF power, ICP RF power, DC-bias, base pressure, process pressure and etch gases. The range of the factors that can be tuned is given in the table below. The available process gases are Cl_2, $SiCl_4$, CH_4, H_2, Ar, O_2, Nf_3, N_2O, N_2, SiH_4.

Table 3.1: Factors that can be attuned in the ICP tool.

Parameter	Minimum Value	Maximum Value
ICP power	0 W	2000 W
Forward power	0 W	500 W
Process pressure	1 mTorr	99 mTorr
Chlorine flow rate	0 sccm	50 sccm
Argon flow rate	0 sccm	50 sccm

Volatility of the etch by-products is a crucial factor in determining the etch rate, as the removal of etch by-products is necessary for further etching of the substance. A lower boiling point may imply higher volatility [24]. The literature lacked data on existing etching recipes suitable for the required dimension scale. Additionally, the numerous factors involved rendered the number of necessary experiments greater

than what could be feasibly conducted within the allocated time and resources. The approach taken to circumvent this challenge was to identify the existing recipes for etching materials and modify them by comparing the bond strength of the material.

Various experiments in the literature show that Cl-based plasma, mainly Cl_2 and Ar-based reactive ion etching was the top choice for the etching of AlN and AlGaN [22, 25, 26, 27, 28, 29, 30, 31, 32, 33, 34]. While issues like lack of information on dimensions were etched, the recipes discussed served as a good starting point for the series of experiments. The most relevant issue is the fact that the nickel mask used in the dry etch process needs to be reused, hence the recipe that provides the best etch profile also needs to corrode the nickel layer to the minimum. The details of the experiments run on the 6 samples of the first batch of experiments are summarized in Table 6.1. The tool only allowed the user to manipulate the flow rates, ICP power, forward power, maximum chamber pressure value, and etch time. The DC voltage is self-biased, hence the changes were only just monitored and noted down.

An etch rate value higher than 75 nm/minute has been reported to increase the surface roughness [35]. The parameters in the same reference whose values resulted in the 75 nm/minute etch rate were used as the baseline. The baseline values were selected as ICP power = 100 W, forward power = 100 W and the percentage of Chlorine in the process gas was kept at 60% of the total composition. During this run of experiments, ICP power was kept to 0 W. The first two samples were etched with different forward power to understand the influence of the forward power on the selectivity and etch rate. Then the Cl_2 percentage was increased to understand the changes as the gas composition percentage changes in the third and fourth samples. Since $SiCl_4$ was also available as the process gas, one of the samples was used to test the effect of this gas, with low forward and ICP power to understand the influence of the gas and see if its feasible gas chemistry. The ICP RIE etch method was also done using just Cl_2 as the process gas. This enables chemical dry etching. The same setup for Cl_2/Ar based plasma etching was used. Ion milling is done using chlorine ions beam current of 30 mA, beam voltage of 500 V, neutralizer current of 30 mA and acceleration voltage of 300 V for 4 minutes.

3.2.2 Wet etching

It is reported that wet etching of AlGaN with strong bases like potassium hydroxide(KOH) aqueous solution and tetramethylammonium hydroxide (TMAH) can introduce m-plane and r-pane facets and is slow as well as the etch [36]. It is reported that the etching of AlN using HF does not meet our requirements [26]. A combination of wet and dry etching is a possibility to be explored. Hence our experiments involved the use of wet etching in combination with dry etching to see the improvement in surface roughness and etch profile quality [36].
TMAH is a strong base that has been shown to etch 3 um thick ALN film grown on a c-plane sapphire substrate with a 16.5 nm per minute etch rate. Hence a time series wet etching of 5,10 and 15 minutes will be done. TMAH was chosen as it was most accessible to our set of experiments.

3.3 Characterization

While the preferred structure is cylindrical air holes in the AlN layer, to enable successful characterization stripes of varying width have been used as the pattern to conduct experiments of etching. The samples required extensive characterization to understand the effects of different processing. To understand the etch profiles, the sample needed to be cleaved to be analyzed by Scanning Tunneling Microscopy(SEM). The factors relevant to understanding the quality of the etch process are etch rate, selectivity, anisotropy, and hand homogeneity. Etch rate is the speed of the process given by

$$R = d/t_{etch}(\text{Å}/minute) \tag{3.1}$$

where t_{etch} is the time for which the material has been subjected to etching, and d is the distance etched. Selectivity is the ratio of etch rates. Anisotropy is given by the equation

$$A = 1 - (R_{horizontal}/R_{vertical}) \tag{3.2}$$

where R is the etch rate. Since in these experiments, the characterization method to understand etch depths is not reliable for horizontal direction, anisotropy is not calculated and is disregarded as a factor for consideration. The uniformity of the etch rate is calculated by

$$U = (R_{high} - R_{low})/(R_{high} + R_{low}) \tag{3.3}$$

here the R_{high} is the etch rate calculated by using the highest value of etch depth measured on the sample and R_{low} is the etch rate calculated by using the lowest value of etch depth measured on the sample.

3.3.1 Profilometer

For measuring the nickel layer thickness before and after etching, a surface profilometer with a 2.5-micron wide stylus is used. To calculate the AlGaN and Ni etch depth, the structure was measured immediately after etching and then after removing the Ni layer. This was to obtain values d_2 and d_4 as depicted in Figures 3.3 and 3.4. The order in which the etch rate calculation is done is outlined in Figures 3.2, 3.3, and 3.4.

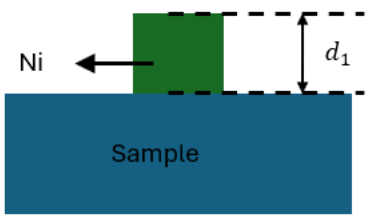

Figure 3.2: Structure with Ni deposited before etching, d_1=75 nm.

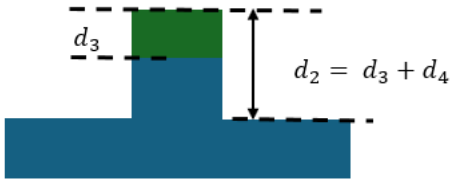

Figure 3.3: Structure with measured after etching, d_2 is measured.

Figure 3.4: Structure after etching with Ni removed, d_4 measured.

This was used to calculate the etch depth in the Ni layer and the AlGaN layer. The amount of AlGaN etched is equal to d_4 and the amount of nickel etched is equal to d1-d3 which is calculated as

$$d_1 - d_3 = d_1 - (d_2 - d_4) \tag{3.4}$$

The etch rate, R, can be calculated as

$$R_{AlGaN} = d4/t_{etch} \tag{3.5}$$

$$R_{Ni} = (d1 - d3)/t_{etch} \tag{3.6}$$

where t_{etch} is the etch time.

3.3.2 Scanning electron microscopy

After etching the samples are stripped of the nickel layer, cleaved, and examined using SEM. SEM uses a beam of electrons for surface scanning. The electrons generated from the electron gun are passed through several electromagnetic guns to condense the electrons to a fine probe for scanning. The image is obtained by two phenomena- the backscattering of electrons (BSE) and the emission of secondary electrons (SE). BSE is used to get good chemical contrasts while SE is used to get good topological contrast as more electrons escape from topological surfaces than flat surfaces. While BSE and SE give topological contrast, SE is the primary signal. Area with atoms of higher atomic number will appear brighter. When the acceleration voltage increases, the wavelength of the electrons decreases, which reduces probe size which results in finer probing. A higher acceleration voltage can cause a larger interaction zone in the lateral direction which can reduce lateral spatial resolution. Hydrocarbon-containing specimens leave a dark mark after examining with higher

resolution [37]. Since the sample has an insulating layer on top after Ni is removed, a low working distance and electron gun power in the range of 1-5kV is used. A 6 nm gold layer was sputtered on the sample as AlN is an insulator and for good quality SEM images the surface needs to be conductive.

4

Results and Discussions

The experiments were run in six batches to test out various parameters. All the batches have a nickel layer thickness of 75 nm. The experiments focused on optimizing the dry etch process. Wet etching experiments were also done to understand the possible wet etchants and their impact on the structure. The results are divided into preliminary tests which tried to replicate etching recipes from the literature, ICP power influence study, RF power influence study and gas chemistry influence study.

4.1 Dry etching

ICP RIE etching was done on samples to understand the influence of ICP power, forward power, and etch gas chemistry on the etch rate of AlGaN, etch rate of Ni, selectivity, surface roughness, sidewall angle and etch rate uniformity across the profile. Ion milling experiments were tested out but the process damaged the samples, hence further experiments with the process were not tested out. The values of parameters which was selected as the baseline for the experiments are detailed in Table 4.1 and the conclusions arrived at by analysing the recipes from the literature are summarized in Table 4.2. Since AlN is a piezoelectric material it has been widely used in MEMS devices, hence literature review on the fabrication of such devices served as a baseline for the experiments.

Table 4.1: Preliminary test parameters for dry etch process.

Sample No	Flow Rate (sccm)			ICP Power (Watts)	Forward Power (Watts)	DC Bias (Volt)	Etch Time (Minutes)
	Ar	Cl2	SiCl4				
1	15	30		0	50	200	12
2	15	30		0	100	329	7
3	15	50		0	100	350	7
4	15	50		0	50	200	12
5	20		10	55	30	246	5

The SEM images are used to understand the etch profile, etch depth, etch width at the top and bottom, uniformity of the etch profile over the sample, and surface roughness. The SEM images and Table 4.2 summarizes the comments.

Table 4.2: Prelimenary test SEM analysis summary.

Sample number	Etch depth (nm)	Etch width -top (nm)	Etch width -bottom (nm)	Undercut angle (degrees)	Etch profile uniformity	Surface damage
1	161.5	98.67	-	102.3	uniform	minimum
2	200.9	126.7	-	104	uniform	minimum
3	416	128.1	30.08	-	-	damage seen on stripes
4	359.5	107	32.54	-	extreme variations seen across profile	contamination high
5	22.58	85.19	47.53	-	uniform	extremely damaged

The preliminary tests showed $SiCl_4$ is not a promising candidate as the process gas since it showed build-up on the surface which could be due to the comparatively involatile etch by-products. The higher RF power showed high DC bias. An increase in the Cl_2 percentage showed higher damage to the surface while increased RF power did not show any considerable change even with higher etch time. The data is insufficient to be conclusive about any assumptions made after the first test. The flow rate was fixed to 15 sccm Ar and 30 sccm Cl_2 after the first run. Etch rate analysis was not done on the preliminary batch. The results from these tests were used to determine the starting parameters for the ICP power influence study conducted summarized in Table 4.3.

4.1.1 Influence of ICP power on AlGaN and Ni etch process

To understand the influence of ICP power on the etch rate of AlGaN and nickel, ICP power was tested from 300 W to 45 W by keeping the forward power, etch time, chlorine flow rate, argon flow rate and chamber pressure constant. The initial experiments indicated that the process might benefit from lower RF power and lower Cl_2 flow rate. During this run, it was noticed that at lower flow rates, the tool couldn't match the input value to the actual value. The mismatch was noticed for ICP power at lower values where the input of 50 W only yielded 45-48 W during the run, with values fluctuating during the process. The DC bias also showed fluctuations increasing with an increase in ICP power. The trends show that even though the AlGaN etch rate consistently increased with increased ICP power, the

Table 4.3: Variation of Ni and AlGaN etch rate with ICP power. The plot shows a linear increase of etch rate till 200 W for the AlGaN etch rate, while the Ni etch rate does not show a similar trend.

Sample No	Flow Rate (sccm)		ICP Power (Watts)	Forward Power (Watts)	DC Bias (Volt)	Chamber Pressure (mTorr)	Etch Time (Minutes)
	Ar	Cl2					
1	10	15	300	80	254-256	-	7
2	10	15	150	80	277	-	7
3	10	15	100	80	290	2.8	7
4	9.9	14.9	50	79	295-300	2.2	7
5	10	15	69	79	282	2.5	7
6	10	15	21	79	235	2.5	7

Table 4.4: Parameters for the ICP power study.

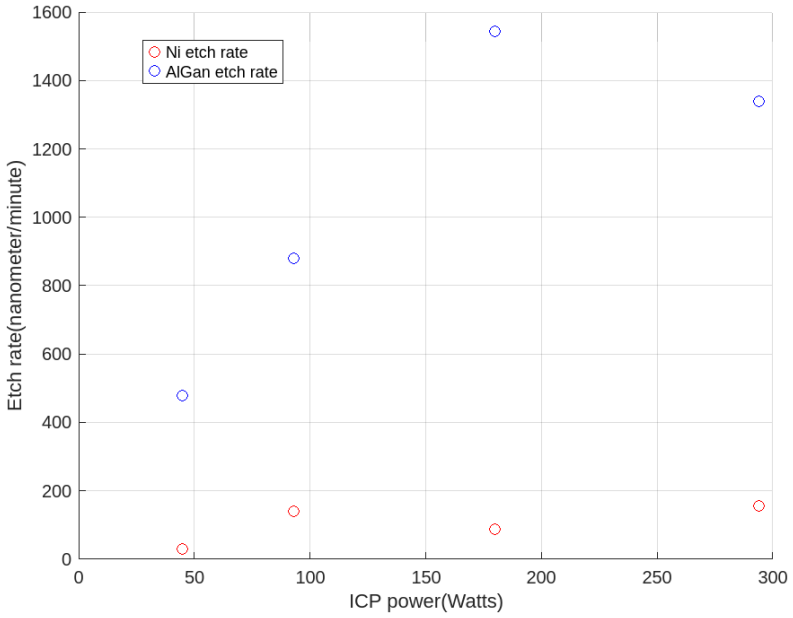

Ni etch rate did not increase with the same scale as depicted in Figure **??**. This could be due to the formation of a nickel oxide layer on the surface due to either the oxygen plasma cleaning step or the ICP RIE etch process itself. The profilometer measurements showed that for the samples which were etched with more than 100 W ICP power the nickel layer thickness increased. While Ni and NiO both arrange themselves in a face-centred cubic lattice, the lattice constant of NiO is higher, this could be the reason for the apparent increase of the nickel layer. No conclusive evidence of the dependence of ICP power on the etch selectivity could be found as depicted in Figure 4.1. The SEM images were used to understand the etch profile, etch depth, etch width at the top and bottom, uniformity of the etch profile over the sample, and surface roughness. The SEM evaluation showed ICP power did not show considerable influence on profile shape, but only on etch depth.

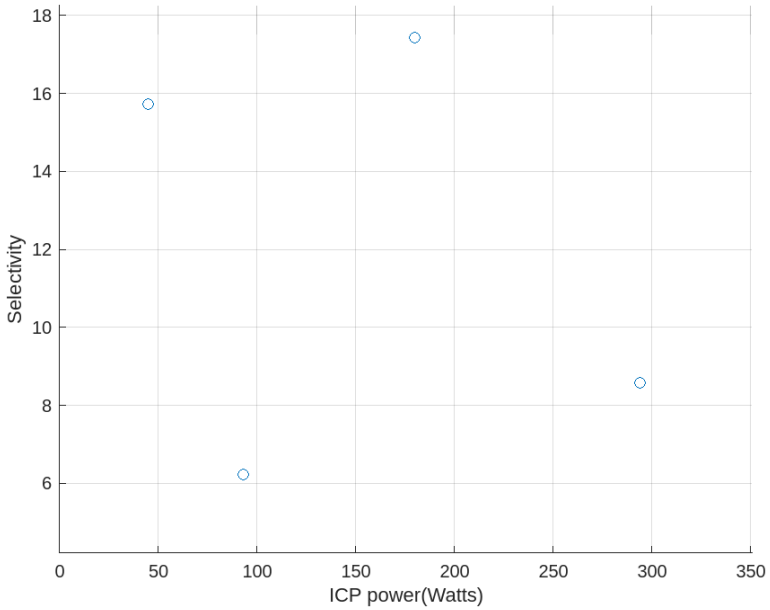

Figure 4.1: Etch selectivity as a function of ICP.

4.1.2 Influence of forward power on AlGaN and nickel etch process

The forward power was varied to understand the influence of the same by keeping the other parameters constant. The etch rate of AlGaN and Ni with respect to different RF power is plotted in Figure 4.2. Forward power 50 W showed the highest selectivity while SEM images of samples treated with lower than 50 W showed increased surface roughness. As RF power increases implies higher DC bias which may enable ion bombardment, hence higher selectivity. However, after the peak at 50 w as depicted in Figure 4.3 selectivity decreases, this could be because as RF power increases the diffusion of plasma particles decreases which reduces chemical etching. Selectivity typically increases with chemical reactions between particles and the material to be etched.

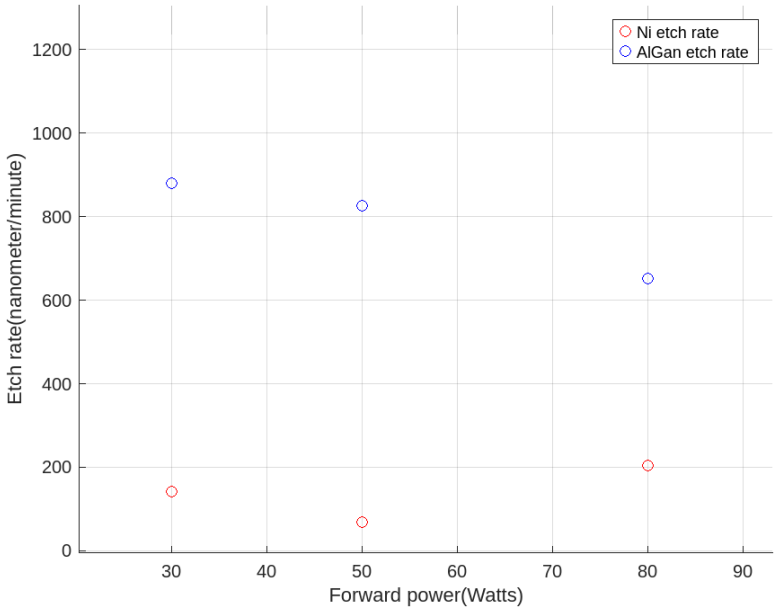

Figure 4.2: Variation of Ni and AlGaN etch rate with forward power. The plot shows a linear decrease in the etch rate for AlGaN with increasing forward power and no trend for the etch rate of Ni.

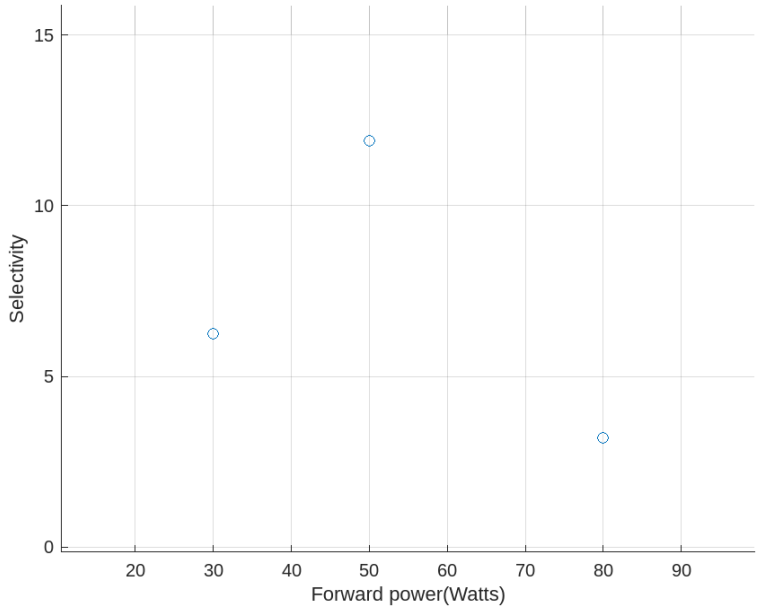

Figure 4.3: The variation of selectivity shows that the forward power of 50 W has the highest selectivity.

4.1.3 Gas chemistry influence study

The influence of different gas compositions was tested while keeping the ICP, forward power constant, and etch time constant. The etch time was decreased to 3 minutes. Forward power was reduced to 50 W and ICP power was kept at 100 W. The chamber pressure at 5 mTorr. The total flow rate to the chamber was kept constant at 50 sccm. 100% chlorine and 50% chlorine in the total gas flow rate were inspected for

surface roughness. The experiments showed that the etch depth and profile across the sample were not as uniform as expected. Variations were observed in the etching behaviour of the full chlorine process for stripes on the same substrate as depicted in Figure 4.4. In contrast, this was not observed with mixed chemistry processes. The fully chlorine-based process showed high selectivity but the profiles were not similar across different stripes on the same sample. This could be due to the exhaustion of the process gas as the effective area of etching is high. The layout is such that the nickel mask only covers a small portion of the total structure. This could lead to the gas being exhausted before it reaches the sides of the substrate, as the SEM analysis showed the etch depth at the centre is higher than at either side of the substrate. Since increasing the total gas flow showed greater damage done to the substrate, increasing the presence of a mask over the surface area might be a good step toward improving a fully chlorine-based plasma process. Figures 4.5 and 4.6 are the SEM

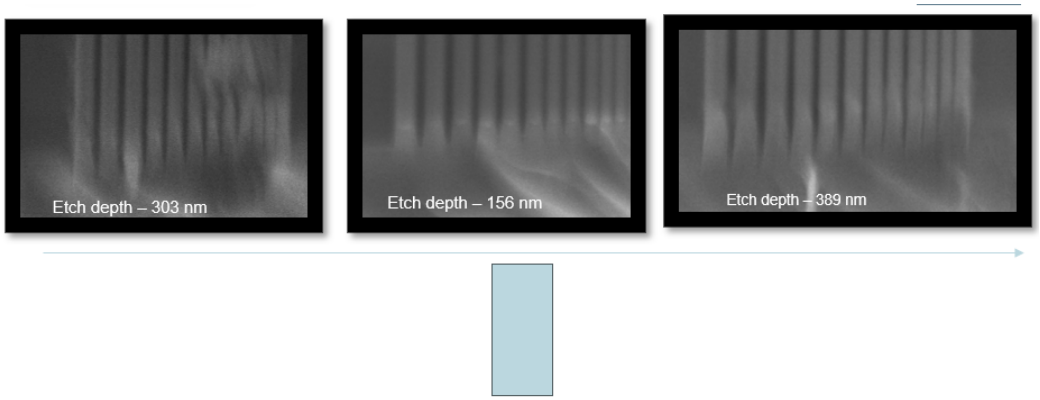

Figure 4.4: Comparision of etch depth variation on different grating on the same sample. Grating on the edges of the sample had higher etch depth while grating at the centre had lower etch depth. The blue rectangle depicts the substrate.

images for the 100% chlorine in the etchant gas composition and Figures 4.7 and 4.8 for the 50% chlorine. For all the other parameters kept constant, the 50% chlorine mixture shows the cross-section profile to be smoother.
The results showed that ICP power and RF power were not as crucial as chlorine flow rate percentage to surface roughness. It was observed that while it is possible to etch AlGaN deep, the side wall angle and surface roughness differed with the chlorine flow rate For a uniform etch profile over the surface, the chlorine percentage had to be kept low, and for high selectivity, the chlorine percentage needed to be high. The best-assumed findings from the study are that since the mask coverage on the substrate is low, the process gas gets consumed easily and hence just using chlorine-based chemical etching without ion-based sputtering provided by the argon molecules, the etch profile turns out to be non-uniform. However, using a higher argon percentage decreases the selectivity and hence chlorine is required in the etch gas mixture. The need for higher RF power could be because AlN is a chemically inert molecule. ICP power only influenced the etch rate, as the ICP power increased the etch rate increased, however, the selectivity was the highest in the 150 W to 50 W range. RF power 50 W and ICP power 100 W with a 1:1 ratio of Cl and Ar in the

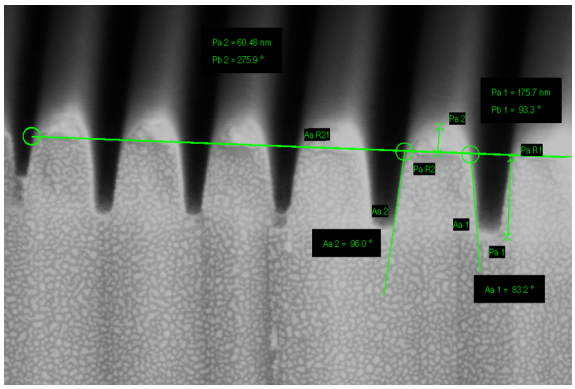

Figure 4.5: 100% chlorine-based ICP RIE, surface coated with 6nm Au for better visibility. Sidewall angle is 96^0-83.2^0 with vertical etch depth 175.7 nm and width at the top 60.48 nm

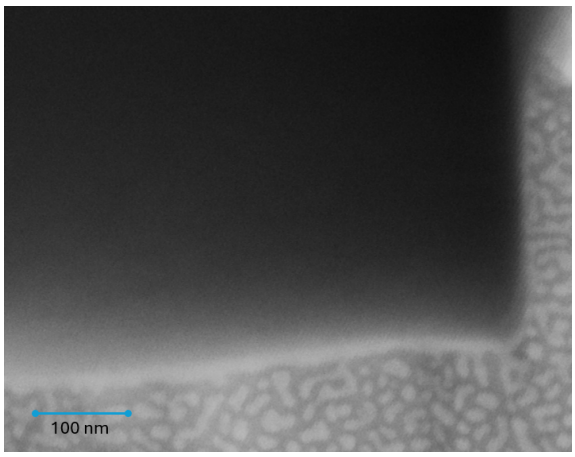

Figure 4.6: Zoomed in cross-section of the surface shows roughness for 100% chlorine based ICP RIE.

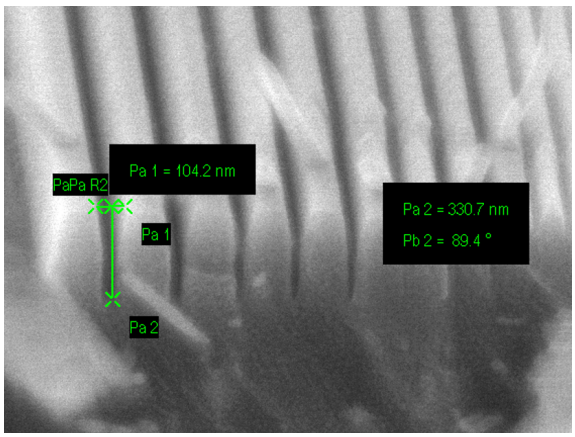

Figure 4.7: Profile of samples etched with 50% chlorine. Vertical etch depth 330.7 nm and width at the top 104.2 nm.

total flow rate showed comparatively smoother profiles while etching the required depth. Lower RF power showed a rougher surface. To conclude, a total flow rate

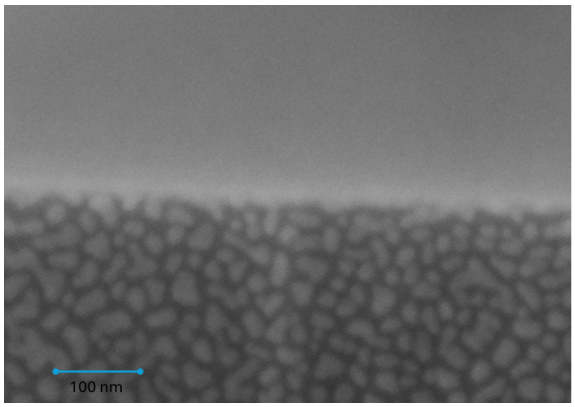

Figure 4.8: Cross section of the sample etched with 50% chlorine.

of 50 sccm, with 50% chlorine, Rf power between 30 W - 50 W with ICP power between 75 W and 150 W, was able to etch 300 nm into AlGaN with a vertical profile that could be of interest to UV emitting PCSELs.

4.2 Wet etching

Wet etching with TMAH due to the reasons mentioned in section 3.3 was used to understand the influence on the profile. The substrate which had undergone identical ICP dry etching was left in a bath for 5, 10, and 15 minutes containing ma-D 525 developer without any heat. Ma-D 525 is an aqueous-alkaline TMAH-based developer. All the samples show surface deformity with the irregularities increasing with time as shown in Figure 4.13.

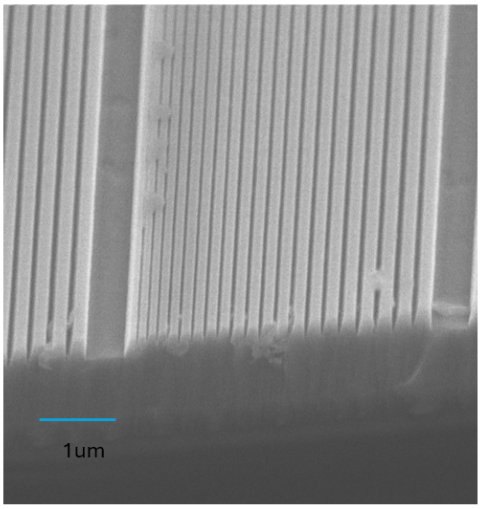

Figure 4.9: a) Dry etched gratings not treated with TMAH.

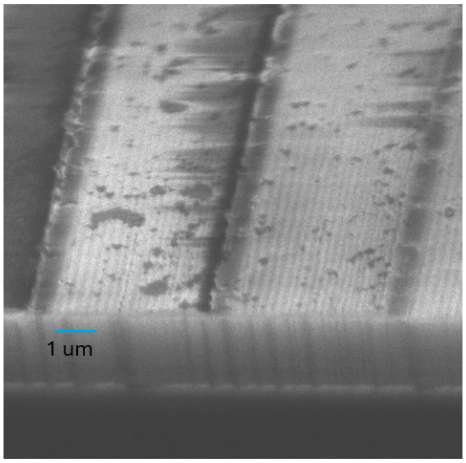

Figure 4.10: b) Sample immersed in TMAH-based developer bath for 5 minutes.

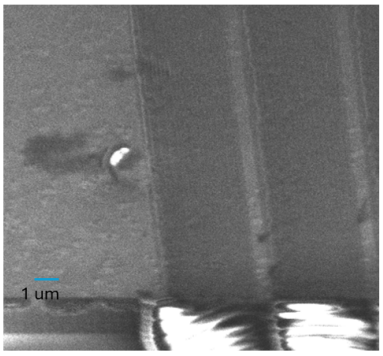

Figure 4.11: c) Sample immersed in TMAH-based developer bath for 10 minutes.

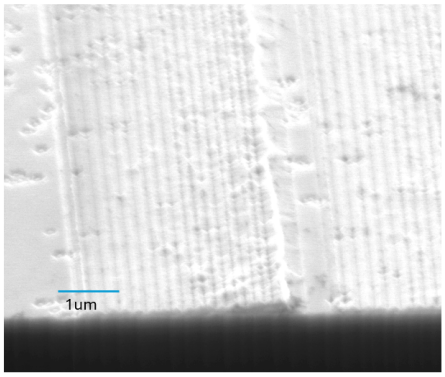

Figure 4.12: d) Sample immersed in TMAH-based developer bath for 15 minutes.

Figure 4.13: TMAH treated samples show wet etching is not vertical but rather shows no significant trend.

5

Future Work and Conclusion

The study involved understanding the working of UVC PCSELs and analyzing different possible etching mechanisms including dry etching and wet etching. Concerning different dry etching techniques, ICP-RIE etching was a suitable process. Even though we have been able to etch the desired structure the full influence of the parameters couldn't be mapped due to limitations in sample numbers and the number of experiments that could have been run within the given time. The study concludes at the point that ICP-RIE etching using Chlorine and Argon, with 50% chlorine in a 50 sccm total gas flow, with 100 W ICP power and 50 W RF power was able to etch AlGaN structures of 300 nm depth with nickel mask. Etch selectivity increased with increasing Cl percentage in the total flow rate but the etched metal surface was rougher. There was less lateral etch uniformity with increasing Cl percentage which was observed by the difference in etch rate at larger structures on the sample and the etch rate observed in the photonic crystal in the cross-section SEM images. The highest Cl% led to a rougher etched AlGaN/AlN surface. More substantial tests into understanding the influence of etching on the nickel layer need to be executed, to actualize electrical injection. The challenges encountered in characterizing the samples, particularly due to the difficulties in cleaving AlN on sapphire, have impacted the evaluation of photonic crystal structures. However, overcoming these challenges is crucial, as the results will directly contribute to the development of UV PCSELs, enabling more efficient and precise laser performance in the ultraviolet spectrum.

References

[1] M. Martín-Sómer, C. Pablos, R. van Grieken, and J. Marugán, "Influence of light distribution on the performance of photocatalytic reactors: LED vs mercury lamps," *Appl. Catal. B*, vol. 215, pp. 1–7, Oct. 2017.

[2] A. Einstein, "Zur quantentheorie der strahlung (on the quantum theory of radiation)," *Physika Zeitschrift*, vol. 18, pp. 121–128, 1917.

[3] M. Y. J. G. M. D. Z. Susumu Noda, Takuya Inoue and K. Ishizaki, "High-power and high-beam-quality photonic-crystal surface-emitting lasers: a tutorial," *Adv. Opt. Photon.*, 2023.

[4] M. Kneissl, "A brief review of iii-nitride uv emitter technologies and their applications," in *III-Nitride Ultraviolet Emitters*, Springer Series in Materials Science, pp. 1–25, Cham: Springer International Publishing, 2016.

[5] K. Iga, "Surface-emitting laser - it's birth and generation of new optoelectronics field," *Selected Topics in Quantum Electronics*, vol. 6, pp. 1201–1215, 2000.

[6] D. J. Elliott, "Ultraviolet light," in *Ultraviolet Laser Technology and Applications*, pp. 1–32, Elsevier, 1995.

[7] N. Taguchi, A. Iwai, M. Noguchi, H. Takahashi, A. Michiue, M. D. Zoysa, T. Inoue, K. Ishizaki, and S. Noda, "Green-wavelength gan-based photonic-crystal surface-emitting lasers," *Applied Physics Express*, vol. 17, no. 1, p. 012002, 2024.

[8] S. Noda, "Progressing the photonic-crystal surface-emitting lasers," *Compound Semiconductor*, vol. 28, no. 6, 2022.

[9] K. Emoto, T. Koizumi, and M. e. a. Hirose, "Wide-bandgap gan-based watt-class photonic-crystal lasers," *Communications Materials*, vol. 3, p. 72, 2022.

[10] *Advances in UV Spectroscopy for Monitoring the Environment*, vol. 3. Benedict & Extension, Kiu Publication, 2024.

[11] H. Y. Lu, S. C. Tian, C. Z. Tong, and et al., "Extracting more light for vertical emission: high power continuous wave operation of 1.3-μm quantum-dot photonic-crystal surface-emitting laser based on a flat band," *Light: Science & Applications*, vol. 8, p. 108, 2019.

[12] R. J. E. Taylor, D. M. Williams, J. R. Orchard, D. T. D. Childs, S. Khamas, and R. A. Hogg, "Band structure and waveguide modelling of epitaxially regrown photonic crystal surface-emitting lasers," *Journal of Physics D: Applied Physics*, vol. 46, no. 26, p. 264005, 2013.

[13] V. Mizeikis, S. Juodkazis, A. Marcinkevičius, S. Matsuo, and H. Misawa, "Tailoring and characterization of photonic crystals," *J. Photochem. Photobiol. C: Photochem. Rev.*, vol. 2, pp. 35–69, July 2001.

[14] A. Larsson, *Semiconductor Optoelectronics-Device Physics and Technologies*. Chalmers Library, n.d.

[15] User:Ddnqt, "Dimensions of photonic crystal." https://commons.wikimedia.org/wiki/File:Dimensionphc.png, 2007. Wikimedia Commons.

[16] L. Thylén, M. Qiu, and S. Anand, "Photonic crystals–a step towards integrated circuits for photonics," *Chemphyschem*, vol. 5, no. 9, pp. 1268–1283, 2004.

[17] E. Strandberg, "Design of a photonic-crystal surface-emitting laser for emission in ultra-violet," Master's thesis, Chalmers university of technology, Gothenburg, Sweden, 2021.

[18] t. i. I. Daniel Mayer, "Hexagonal crystal structure." https://commons.wikimedia.org/wiki/File:Hexagonal_lattice.svg, 2007. Wikimedia Commons.

[19] Y. Sugahara, "Aluminum nitride," in *Encyclopedia of Polymeric Nanomaterials*, pp. 1–5, Springer Berlin Heidelberg, 2015.

[20] C. Kittel, *Introduction to Solid State Physics*. Wiley, 8th ed., 2004.

[21] S. A. Campbell, *Fabrication Engineering at the Micro- and Nanoscale (3rd Edition)*. Oxford University Press, 2008.

[22] R. M. R. Pinto, V. Gund, C. Calaza, K. K. Nagaraja, and K. B. Vinayakumar, "Piezoelectric aluminum nitride thin-films: A review of wet and dry etching techniques," *Microelectronic Engineering*, vol. 257, p. 111753, 2022.

[23] J. W. Coburn and H. F. Winters, "Plasma etching—a discussion of mechanisms," *Journal of Vacuum Science & Technology*, vol. 16, no. 2, pp. 391–403, 1979.

[24] S. Pearton, U. Chakrabarti, and F. e. a. Ren, "New dry-etch chemistries for iii–v semiconductors," *MRS Online Proceedings Library*, vol. 334, pp. 399–411, 1993.

[25] P.-M. Coulon, G. Kusch, P. Fletcher, P. Chausse, R. W. Martin, and P. A. Shields, "Hybrid top-down/bottom-up fabrication of a highly uniform and organized faceted aln nanorod scaffold," *Materials*, vol. 11, p. 1140, 2018.

[26] S. J. Pearton and et al., "Dry and wet etching characteristics of inn, aln, and gan deposited by electron cyclotron resonance metalorganic molecular beam epitaxy," *Journal of Vacuum Science and Technology*, vol. 11, pp. 1772–1775, 1993.

[27] D. Flamm, "Plasma etching for iii-v compound devices: Part i," *Solid State Technology*, p. 77, October 1988.

[28] S. J. Pearton, C. R. Abernathy, F. Ren, J. R. Lothian, P. W. Wisk, and A. Katz, "Dry and wet etching characteristics of inn, aln, and gan deposited by electron cyclotron resonance metalorganic molecular beam epitaxy," *Journal of Vacuum Science & Technology A*, vol. 11, no. 4, pp. 1772–1775, 1993.

[29] "Plasma etching—a discussion of mechanisms." https://pubs.aip.org/avs/jvst/article/16/2/391/842766/Plasma-etching-A-discussion-of-mechanisms. Accessed March 15, 2024.

[30] K. R. Williams, K. Gupta, and M. Wasilik, "Etch rates for micromachining processing-part ii," *Journal of Microelectromechanical Systems*, vol. 12, no. 6, pp. 761–778, 2003.

[31] J. Yang, C. Si, G. Han, M. Zhang, L. Ma, Y. Zhao, and J. Ning, "Researching the aluminum nitride etching process for application in mems resonators," *Micromachines*, vol. 6, no. 2, pp. 281–290, 2015.

[32] X. Liu, C. Sun, B. Xiong, L. Niu, Z. Hao, Y. Han, and Y. Luo, "Smooth etching of epitaxially grown aln film by cl2/bcl3/ar-based inductively coupled plasma," *Vacuum*, vol. 116, pp. 158–162, June 2015.

[33] V. Bliznetsov, B. H. B. Johari, M. T. Chentir, W. H. Li, L. Y. Wong, S. Merugu, X. L. Zhang, and N. Singh, "Improving aluminum nitride plasma etch process for mems applications," *Journal of Micromechanics and Microengineering*, vol. 23, no. 11, p. 117001, 2013.

[34] H. Cho, C. B. Vartuli, C. R. Abernathy, S. M. Donovan, S. J. Pearton, R. J. Shul, and J. Han, "Cl2-based dry etching of the algainn system in inductively coupled plasmas," *Solid-State Electronics*, vol. 42, no. 12, pp. 2277–2281, 1998.

[35] V. Kuryatkov, B. Borisov, J. Yun, G. Kipshidze, S. Nikishin, H. Temkin, D. Aurongzeb, and M. Holtz, "Evolution of surface roughness of aln and gan induced by inductively coupled cl/ar plasma etching," *Journal of Applied Physics*, vol. 95, 2004.

[36] S. Yasue, K. Sato, Y. Kawase, J. Ikeda, Y. Sakuragi, S. Iwayama, M. Iwaya, S. Kamiyama, T. Takeuchi, and I. Akasaki, "The dependence of aln molar fraction of algan in wet etching by using tetramethylammonium hydroxide aqueous solution," *Japanese Journal of Applied Physics*, vol. 58, p. SCCC30, 2019.

[37] Y. Leng, *Materials Characterization*. Wiley, 2013.

[38] W. Meredith, "The international symposium on blue lasers & LEDs," *111-Vs Rev.*, vol. 9, pp. 56–58, June 1996.

[39] K. Emoto, T. Koizumi, M. Hirose, M. Jutori, T. Inoue, K. Ishizaki, M. De Zoysa, H. Togawa, and S. Noda, "Wide-bandgap GaN-based watt-class photonic-crystal lasers," *Commun. Mater.*, vol. 3, Oct. 2022.

[40] A. Larsson, "Advances in vcsels for communication and sensing," *IEEE Journal of Selected Topics in Quantum Electronics*, vol. 17, no. 6, pp. 1552–1567, 2011.

[41] M. Imada, S. Noda, A. Chutinan, T. Tokuda, M. Murata, and G. Sasaki, "Coherent two-dimensional lasing action in surface-emitting laser with triangular-lattice photonic crystal structure," *Applied Physics Letters*, vol. 75, no. 3, pp. 316–318, 1999.

[42] R. Paschotta, "Photonic crystal surface-emitting lasers." RP Photonics Encyclopedia, 2004. RP Photonics AG.

[43] "A 271.8 nm deep-ultraviolet laser diode for room temperature operation," *IOPscience*. Accessed February 9, 2024.

[44] O. Ambacher, "Growth and applications of group iii-nitrides," *Journal of Physics D: Applied Physics*, vol. 31, no. 20, p. 2653, 1998.

[45] "An electrically injected algan nanowire laser operating in the ultraviolet-c band," *Applied Physics Letters*. AIP Publishing, Accessed February 9, 2024.

[46] P.-M. Coulon, G. Kusch, E. D. Le Boulbar, P. Chausse, C. Bryce, R. W. Martin, and P. A. Shields, "Hybrid top-down/bottom-up fabrication of regular arrays of aln nanorods for deep-uv core–shell leds," *Physica Status Solidi (b)*, vol. 255, no. 5, p. 1700445, 2018.

[47] A. Iqbal and F. Mohd-Yasin, "Reactive sputtering of aluminum nitride (002) thin films for piezoelectric applications: A review," *Sensors*, vol. 18, no. 6, p. 1797, 2018.

[48] J. D. Joannopoulos, S. G. Johnson, J. N. Winn, and R. D. Meade, *Photonic Crystals: Molding the Flow of Light*. Princeton University Press, second edition ed., 2011.

[49] H. Kogelnik and C. V. Shank, "Stimulated emission in a periodic structure," *Applied Physics Letters*, vol. 18, no. 4, pp. 152–154, 1971.

[50] J. K. Lorenz, E. Baer, A. Burenkov, A. Erdmann, P. Evanschitzky, and P. Pichler, "Challenges and opportunities for process modeling in the nanotechnology era," *Journal of Computational Electronics*, vol. 13, no. 1, pp. 3–17, 2014.

[51] M. Meier, A. Mekis, A. Dodabalapur, A. Timko, R. E. Slusher, J. D. Joannopoulos, and O. Nalamasu, "Laser action from two-dimensional distributed feedback in photonic crystals," *Applied Physics Letters*, vol. 74, no. 1, pp. 7–9, 1999.

[52] R. Miyagawa, J. Wu, H. Miyake, and K. Hiramatsu, "Growth of high quality c-plane aln on a-plane sapphire," *MRS Online Proceedings Library*, vol. 1202, no. 1, p. 502, 2020.

[53] J. F. Muth, J. D. Brown, M. A. L. Johnson, Z. Yu, R. M. Kolbas, J. W. Cook, and J. F. Schetzina, "Absorption coefficient and refractive index of gan, aln and algan alloys," *MRS Internet Journal of Nitride Semiconductor Research*, vol. 4, no. 1, pp. 502–507, 1999.

[54] S. Nakamura, "Light emission moves into the blue," *Physics World*, vol. 11, no. 2, p. 31, 1998.

[55] D. R. Paschotta, "Photonic crystal surface-emitting lasers." https://www.rp-photonics.com/photonic_crystal_surface_emitting_lasers.html. Accessed February 14, 2024.

[56] K. Racka-Szmidt, B. Stonio, J. Żelazko, M. Filipiak, and M. Sochacki, "A review: Inductively coupled plasma reactive ion etching of silicon carbide," *Materials*, vol. 15, no. 1, 2022.

[57] "Sensors free full-text reactive sputtering of aluminum nitride (002) thin films for piezoelectric applications: A review." https://www.mdpi.com/1424-8220/18/6/1797. Accessed February 27, 2024.

[58] T. D. Thangadurai, N. Manjubaashini, S. Thomas, and H. J. Maria, "Fabrication of nanostructures," in *Nanostructured Materials* (T. D. Thangadurai, N. Manjubaashini, S. Thomas, and H. J. Maria, eds.), pp. 129–147, Cham: Springer International Publishing, 2020.

[59] B. T. Tran, N. Maeda, M. Jo, D. Inoue, T. Kikitsu, and H. Hirayama, "Performance improvement of aln crystal quality grown on patterned si(111) substrate for deep uv-led applications," *Scientific Reports*, vol. 6, p. 35681, 2016.

[60] OpenAI, "Chatgpt (4o) [large language model], the author admits to using chatgpt to help structure sentences sometimes.," 2024.

[61] M. Gustaver, "A chalmers university of technology master's thesis template for ," 2020. Unpublished.

DEPARTMENT OF SOME SUBJECT OR TECHNOLOGY
CHALMERS UNIVERSITY OF TECHNOLOGY
Gothenburg, Sweden
www.chalmers.se

CHALMERS
UNIVERSITY OF TECHNOLOGY